Icarus 300 (2018) 12–20

Contents lists available at ScienceDirect

Icarus

journal homepage: www.elsevier.com/locate/icarus

Arecibo and Goldstone radar images of near-Earth Asteroid (469896) 2005 WC1

Kenneth J. Lawrence[a,*], Lance A.M. Benner[a], Marina Brozovic[a], Steven J. Ostro[a], Joseph S. Jao[a], Jon D. Giorgini[a], Martin A. Slade[a], Raymond F. Jurgens[a], Michael C. Nolan[b], Ellen S. Howell[b], Patrick A. Taylor[c]

[a] Jet Propulsion Laboratory, California Institute of Technology, Pasadena, CA 91109-8099, USA
[b] Lunar and Planetary Laboratory, University of Arizona, Tucson, AZ 85721-0092, USA
[c] Arecibo Observatory, Universities Space Research Association, Arecibo, Puerto Rico, 00612, USA

ARTICLE INFO

Article history:
Received 16 May 2017
Revised 18 August 2017
Accepted 22 August 2017
Available online 26 August 2017

Keywords:
Radar observations
Near-Earth asteroids
Asteroid rotation
Asteroid surfaces

ABSTRACT

We report radar observations of near-Earth asteroid (469896) 2005 WC1 that were obtained at Arecibo (2380 MHz, 13 cm) and Goldstone (8560 MHz, 3.5 cm) on 2005 December 14–15 during the asteroid's approach within 0.020 au The asteroid was a strong radar target. Delay-Doppler images with resolutions as fine as 15 m/pixel were obtained with 2 samples per baud giving a correlated pixel resolution of 7.5 m. The radar images reveal an angular object with 100 m-scale surface facets, radar-dark regions, and an estimated diameter of 400 ± 50 m. The rotation of the facets in the images gives a rotation period of ~2.6 h that is consistent with the estimated period of 2.582 h ± 0.002 h from optical lightcurves reported by Miles (private communication). 2005 WC1 has a circular polarization ratio of 1.12 ± 0.05 that is one of the highest values known, suggesting a structurally-complex near-surface at centimeter to decimeter spatial scales. It is the first asteroid known with an extremely high circular polarization ratio, relatively low optical albedo, and high radar albedo.

1. Introduction

Near-Earth asteroid (NEA) 2005 WC1 was discovered by the Lincoln Near-Earth Asteroid Research (LINEAR) program on November 21, 2005 (MPEC 2005-W36, http://www.minorplanetcenter.net/mpec/K05/K05W36.html). The Minor Planet Center classified it as a "potentially hazardous asteroid" (PHA). With a semi-major axis of 1.40 au, eccentricity of 0.49, and inclination of 20.0°, 2005 WC1 is in the Apollo family. 2005 WC1 crosses the orbit of Mars, and with a perihelion distance of 0.719 au, it also crosses the orbit of Venus. Its absolute magnitude of 20.7 (https://ssd.jpl.nasa.gov/sbdb.cgi?sstr=2005%20WC1) suggests a diameter within a factor of two of 0.25 km. No formal absolute magnitude error estimate is available and the error may be as large as several tenths of a magnitude. A few weeks after discovery, 2005 WC1 made a close approach to the Earth at 0.020 au (7.7 lunar distances) on December 14.

Higley et al. (2008) reported clear filter photometry obtained at the Badlands Observatory on 2005 December 13, one day before the flyby. The lightcurve clearly shows brightness increases of at least 1.3 magnitudes twice in the same night. A period of approximately 2 hours was determined with an enormous amplitude of nearly two magnitudes. About one week earlier, Miles (2008) reported a period of 2.57 ± 0.02 h based on three complete revolutions during a 9 h observing run at Golden Hill Observatory, but measured a significantly different amplitude of 0.5 magnitudes. The discrepancies between the two observers in the lightcurve amplitudes may be due to the difference in the subobserver latitude and/or the 45° of sky motion between the observations, resulting in solar phase angles of 88° at the time of the Higley observations versus 49° for the observations reported by Miles. A refined period of 2.582 ± 0.002 h was estimated by Miles (private communication) from three nights of data. Throughout this paper, we adopt the 2.582 h value. We are unaware of any visual or infrared spectroscopy for this object.

During the warm mission of the Spitzer Space Telescope, 2005 WC1 was observed on 2009 August 1 at a heliocentric distance of 1.099 au and a Spitzer-centric distance of 0.259 au (Trilling et al., 2010). Trilling et al. estimated a geometric albedo of 0.11 ± 50% and a diameter of 0.29 km ± 25%.

* Corresponding author.
E-mail address: Kenneth.J.Lawrence@jpl.nasa.gov (K.J. Lawrence).

http://dx.doi.org/10.1016/j.icarus.2017.08.028
0019-1035/

Table 1
Radar observations.

Date	Time UTC	Setup	Resolution μs	Hz	RA (deg)	DEC (deg)	Dist. (au)	OSOD	Runs	$\Delta\phi$ (deg)
Arecibo										
Dec-14	12:59:38 – 13:01:15	CW	–	0.15	217.6	20.0	0.020	14	3	11.7 – 15.5
Dec-14	14:14:54 – 14:15:49	CW	–	0.15				16	2	186.6 – 188.7
Dec-14	14:21:48 – 14:22:43	CW	–	0.15				16	2	202.6 – 204.8
Dec-14	14:25:12 – 14:26:07	CW	–	0.15				18	2	210.5 – 212.7
Dec-14	14:28:15 – 14:28:28	Ranging	4					18	1	217.6 – 218.1
Dec-14	14:29:51 – 14:30:04	Ranging	4					18	1	221.3 – 221.8
Dec-14	14:44:13 – 14:50:20	Imaging	0.1	0.08				18	9	254.7 – 268.9
Goldstone										
Dec-15	13:25:14 – 13:35:10	CW	–	0.5	226.6	−6.1	0.023	22	13	177.4 – 200.5
Dec-15	14:17:41 – 15:30:26	Imaging	0.125	0.25				24	91	299.3 – 108.4

Goldstone and Arecibo radar observations of 2005 WC1. Right ascension (RA), declination (DEC), and geocentric distance are given for each date and observational setup. OSOD is the JPL On-Site Orbit Determination software ephemeris solution number. Runs are the number of transmit and receive cycles. The transmission powers were 450 kW at Goldstone and 440 kW at Arecibo. The rotational phase, $\Delta\phi$, for each observing setup is provided using a rotation period of 2.582 h where the zero-phase epoch is defined as Dec. 14, 2005 00:00:00 UT. All dates refer to 2005.

2. Radar observations

We used the Arecibo and Goldstone radar systems (Ostro 1993) to observe 2005 WC1 as a target of opportunity during its Earth flyby in December 2005. Arecibo transmits in the S-band at a frequency of 2380 MHz (λ = 12.6 cm). Because the Arecibo declination window is limited to within $-1°$ to $+38°$, and due to the rapid motion of the target, in excess of 4000 ″/h, the only day when the asteroid was visible at Arecibo was on December 14. The 70 m antenna at Goldstone operates in the X-band at a frequency of 8560 MHz (λ =3.5 cm) and observed 2005 WC1 on December 15. Table 1 summarizes the observations.

Our radar experiment consisted of a series of transmit and receive cycles slightly less than the duration of the round-trip-time (RTT) for the radar signal to reach and return from the object. Each transmit-receive cycle is called a "run" and can be analyzed as a sum of some whole number of statistically independent measurements or "looks." We use two modes of radar observations during the course of our experiment: continuous waveform (CW) observations that yield echo power spectra, and binary phase coded (BPC) observations that yield ranging measurements and delay-Doppler images. During CW observations, we transmit a circularly polarized electromagnetic wave of constant amplitude and frequency and receive its reflection from the asteroid. The frequency of the reflected wave is shifted by the bulk motion relative to Earth and is dispersed in Doppler frequency due to the object's rotation. The Doppler broadening or bandwidth of the echo is expressed by:

$$B = \frac{4\pi D}{\lambda P}\cos(\delta) \quad (1)$$

where B is the bandwidth of the echo, D is the object's maximum dimension in the plane of sky perpendicular to the radar line-of-sight, P is the rotational period, λ is the radar wavelength, and δ is the sub-radar latitude.

We received the reflected signal from the CW transmissions in the same sense (SC) and the opposite sense (OC) circular polarizations with respect to the outgoing wave. Since single scattering from large, flat surface elements will produce a purely OC echo, the ratio of the echo power strengths in these two polarization channels provides a gauge of the near-surface roughness at spatial scales within an order of magnitude of the radar wavelengths (Ostro 1993; Benner et al., 1997 and Virkki et al., 2014). Among near-Earth and main-belt asteroids, SC/OC is also correlated with some taxonomic classes (Benner et al., 2008 and Shepard et al., 2010). The E and V types tend to have higher polarization ratios compared the other spectral classes.

The BPC mode of observations uses a time-coded waveform that permits the measurement of radar echoes in both Doppler frequency and time-delay. The time-delay resolution is determined by the baud, which is the time interval of switching or not switching the phase of the transmitted waveform (Ostro 1993). We use the BPC observations for ranging measurements and coarse- and high-resolution imaging. We obtain ranging measurements to reduce orbital uncertainties and improve the ephemeris. The highest resolution delay-Doppler images of 2005 WC1 were obtained with a transmitted code resolution of 0.1 μs (15 m). By oversampling the delay-Doppler images in time delay (i.e. obtaining two samples per baud), we obtain a pixel spacing of 7.5 m/row.

3. Orbit determination

The JPL on-site orbit determination (OSOD) solution #14 used at the beginning of the radar experiment was computed from 112 optical observations spanning November 21 – December 11, 2005 and provided good pointing (3-σ uncertainties of 7 arcseconds) for the radar experiment. The initial 3-σ S- and X-band Doppler prediction uncertainties were 140 and 490 Hz. A series of Doppler and ranging corrections to the ephemerides were made throughout the experiment and are summarized in Table 2. The shift in the echo power spectra obtained from Arecibo (Fig. 1A) illustrates the improved accuracy of the different orbit solutions.

Prior to the Arecibo observations, the time interval over which Earth close-approaches could be reliably predicted included only the immediate 2005 discovery apparition. The inclusion of the Arecibo delay-Doppler measurements secured knowledge of the orbit by showing that the next encounter less than 0.1 au from Earth would be in 2063 and increased the overall interval of predictability by 393 years from 1733 to 2126. Adding a second day of radar observations from Goldstone further increased the predictability extent 159 years to 2285. With the current multi-apparition orbit solution (OSOD #40), utilizing the radar astrometry and 209 optical observations from 2005 – 2016, the close approach predictability extends more than 1000 years (Table 3). The discovery apparition is the closest nominal approach within this time period. The close approaches in Table 3 are based on a purely ballistic trajectory that ignores uncertainties in the orbital motion due to the Yarkovsky effect, which has not been detected for this asteroid. It is likely that perturbations due to the Yarkovsky effect will eventually increase the uncertainties more rapidly than suggested by ballistic motion (Vokrouhlicky et al., 2015), which could shrink the interval of orbital predictability. A detailed treatment of the Yarkovsky effect as applied to 2005 WC1 is beyond the scope of this paper.

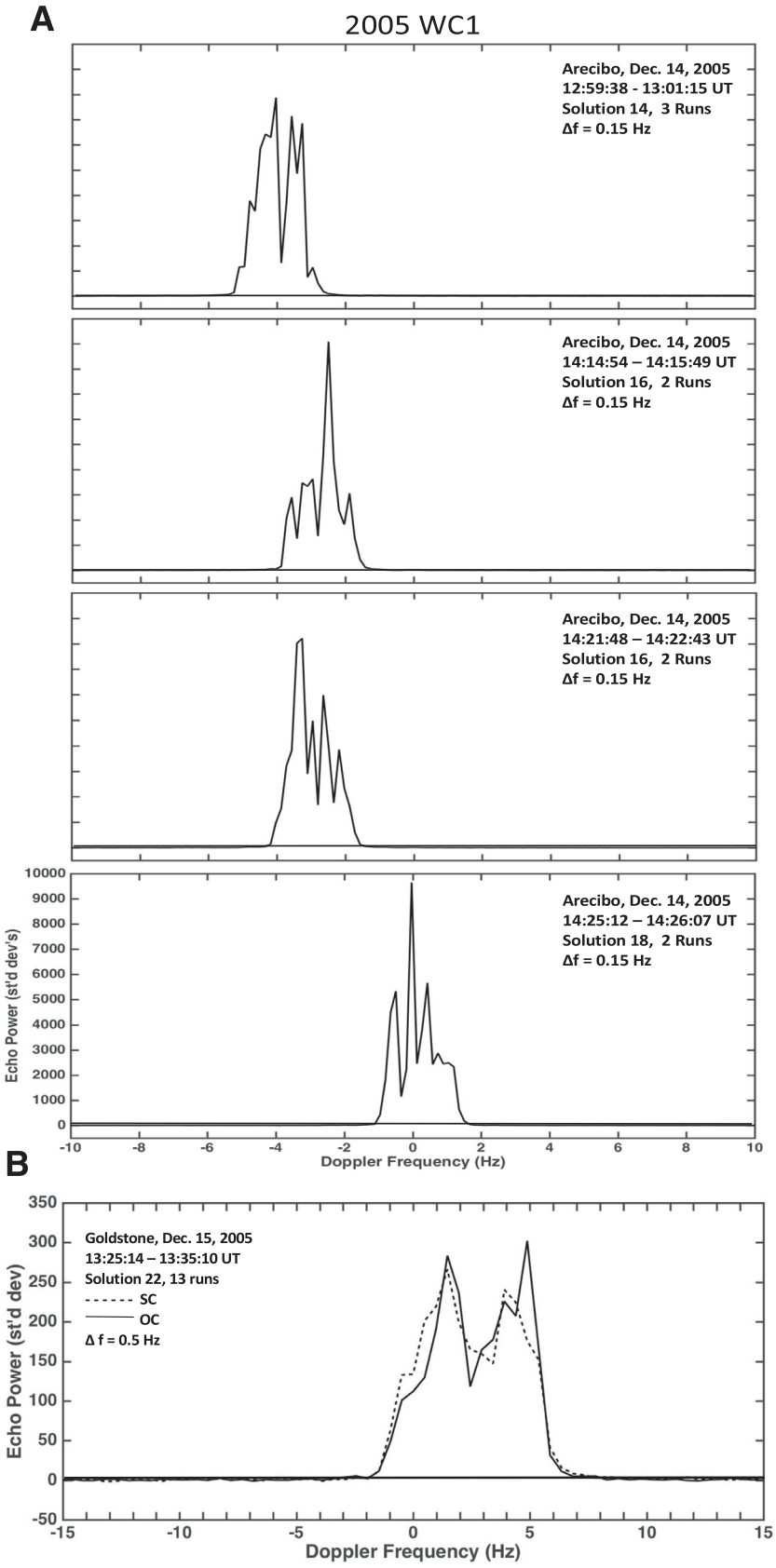

Fig. 1. Arecibo (A) and Goldstone (B) echo power spectra of 2005 WC1. Echo power in standard deviations is plotted as a function of Doppler frequency. The Arecibo and Goldstone frequency resolutions are 0.15 and 0.5 Hz, respectively. These resolutions are close to the same scale when S-band is converted to X-band. Due to equipment problems, the Arecibo spectra are only in the OC channel and there is a 1.25 h gap after the first spectrum was obtained. The offsets from 0 Hz Doppler frequency in Fig. 1A are due to ephemeris uncertainties.

Table 2
Radar astrometry.

Date / Time UTC	Measurement	Correction	Sigma	OSOD	Site
Dec 14 13:00:00	-6206.1020	-4.0 Hz	0.5 Hz	14	Arecibo
Dec 14 14:15:00	-15634.7046	-3.0 Hz	1.0 Hz	16	Arecibo
Dec 14 14:44:00	20198941.39	-331.856 μs	1.0 μs	18	Arecibo
Dec 14 14:44:00	-19261.7405	+0.11 Hz	1.0 Hz	18	Arecibo
Dec 15 13:30:00	-463428.4	+ 3 Hz	1.0 Hz	22	Goldstone

2005 WC1 radar astrometry. Results are also posted on the JPL Solar System dynamics small-body radar astrometry website (http://ssd.jpl.nasa.gov/?radar).

Table 3
Past and future close approaches of 2005 WC1.

Date (TDB)	CA Dist au	MinDist au	MaxDist au	Vrel km/s	TCA3Sg min
1373 Nov 30.97276	0.038043	0.038043	0.050921	17.371	2985.6
1441 Dec 03.13288	0.047228	0.035725	0.087317	16.653	4385.9
1514 Dec 06.11768	0.077595	0.066645	0.089126	15.802	1235.8
1519 Nov 28.84679	0.059876	0.047882	0.073029	18.532	1239.5
1587 Dec 15.46962	0.063923	0.060499	0.067422	16.097	375.98
1592 Dec 07.34928	0.073121	0.068917	0.077369	18.938	367.51
1660 Dec 16.86349	0.090410	0.089276	0.091548	15.456	118.77
1665 Dec 09.35718	0.046726	0.045519	0.047950	18.249	123.14
1733 Dec 10.71064	0.042920	0.042553	0.043289	18.176	36.46
1791 Dec 17.89841	0.077198	0.077047	0.077349	15.703	14.85
1796 Dec 08.33267	0.079126	0.078954	0.079299	19.181	13.76
1854 Dec 17.29309	0.055596	0.055555	0.055637	16.180	3.96
1859 Dec 09.46268	0.093085	0.093038	0.093133	19.559	3.65
1922 Dec 16.49748	0.026605	0.026595	0.026616	16.894	1.21
1927 Dec 10.46939	0.095958	0.095941	0.095975	19.656	1.27
2005 Dec 14.49339	**0.020242**	**0.020242**	**0.020242**	**17.684**	**0.01**
2063 Dec 21.57756	0.095739	0.095727	0.095751	15.211	1.10
2068 Dec 11.68725	0.065006	0.064995	0.065017	18.903	0.82
2097 Jun 03.10976	0.094324	0.094323	0.094324	16.825	0.92
2126 Dec 14.91191	0.036236	0.036185	0.036286	18.179	4.02
2174 Dec 21.36972	0.078030	0.077660	0.078401	15.575	32.14
2203 Jun 07.61996	0.095612	0.095577	0.095647	17.826	4.72
2232 Dec 13.38116	0.080087	0.079525	0.080649	19.293	40.53
2285 Dec 15.15058	0.052869	0.052073	0.053665	18.622	58.54
2309 Jun 08.35288	0.088661	0.088334	0.088996	17.733	52.40
2333 Dec 20.62509	0.029579	0.026526	0.032641	16.640	241.81
2367 Jun 06.92978	0.082864	0.080516	0.091026	16.535	1288.0
2396 Dec 19.42114	0.009276	0.001062	0.066848	17.137	4296.4

Past and future close-approaches to Earth less than 0.10 au for the time-span 1373–2396, bounded by when the 3-sigma encounter distance uncertainty is less than +/− 0.1 au and the 3-sigma encounter time uncertainty is less than +/− 10 days. The nominal close-approach distance, CA Dist, is the geocentric close-approach distance. MinDist and MaxDist are the three-sigma minimum and maximum closest-approach distance possible. The relative velocity, Vrel, of the object and Earth are provided. TCA3Sg is the three-sigma uncertainty in the close-approach time. Results are from a numerical integration that considers point-mass gravity perturbations of the planets, Moon, and the 16 largest asteroids. The Dec. 2005 date, highlighted in bold, is when 2005 WC1 was at its closest approach during of the radar observations. These calculations assume a purely ballistic trajectory and do not include uncertainties in the orbital motion due to the Yarkovsky effect, which probably increases the uncertainties and may reduce the interval of the predictability (Vokrouhlicky et al., 2015). Uncertainties due to the Yarkovsky effect have not been studied for this object.

4. Echo power spectra

Echo power spectra were obtained at each site at the beginning of the observations and are plotted in Fig. 1A and B. Only OC data were collected at Arecibo on December 14 because of equipment issues. In addition, there was a gap of 1.25 h while collecting the CW data. Constraints on the pole-on dimensions can be estimated using Eq. (1), the rotation period, and estimates of the bandwidths. The maximum bandwidth of the Arecibo spectra is 2.7 Hz, which, using P = 2.582 h, places a lower bound on the maximum pole-on dimension of 0.25 km. The bandwidth of the spectra obtained on December 15 from Goldstone is 6.4 Hz, which places a lower bound of 0.17 km on the maximum pole-on dimension. An irregular or elongated shape combined with ~28 deg of sky motion between Dec. 14 and 15 may explain the difference between the two bounds.

Adopting Dec. 14 00:00:00 UT as the zero-phase epoch, we can use the rotation period to compute rotational phases during the experiment (Table 1). We find that the Goldstone CW observations sampled the same rotation phases as those at Arecibo beginning at 14:14:54 on Dec. 15. However, the echo power spectra look very different, possibly because of sky motion or due to a substantial change in the subradar latitude. It is important to note that the Miles period is synodic. There is some uncertainty in the calculated rotation phases because of the rapid motion of the asteroid across the sky. Accurate rotational phases could be obtained by knowing the pole position, but unfortunately, the radar data are insufficient to estimate the pole position.

Fig. 1 shows an echo power spectrum obtained at Goldstone. The spectrum shows a pronounced central dip, and given that the spectrum is a sum of 130 looks, the dip is statistically significant. It may provide evidence for a concavity, a radar albedo feature, or possibly specular reflections. Contact binary asteroids can produce

dips within the CW spectra (Brozovic et al., 2010 and Magri et al., 2011), but there is no evidence from the delay-Doppler images that 2005 WC1 is such an object. The spectrum is not significantly affected by smear because, given the 2.582 h rotation period, the target rotated only 21°. The dip seen in the summed spectra (Fig. 1B) is not consistently seen in the thirteen individual CW spectra. It seems unlikely that it is associated with a topographical feature and is probably a specular glint. In an effort to match the dip seen in the Goldstone spectrum with the Arecibo spectra, we reprocessed the Arecibo CW data at a finer resolution (0.08 Hz) and shifted the last spectrum to correspond to solution 16. The last six runs obtained after 14:14 UT were summed. The results were inconclusive because of the low number of looks and strong self-noise. As a result, the dips and spikes within the Arecibo echo power spectra cannot be interpreted as real features.

Calculated from the Goldstone data, the circular polarization ratio, μ_c or SC/OC, of 2005 WC1 is 1.12 ± 0.05. We adopt an uncertainty slightly larger than that previously published in Benner et al. (2008) due to systematic and calibration errors. This is the second highest published circular polarization ratio of any asteroid measured behind 2003 TH2 at 1.48 ± 0.4 (Benner et al., 2008) and it implies either that the near surface is extremely rough at centimeter to decimeter scales or that some mechanism other than roughness is increasing the polarization ratio. Near surface roughness may involve pits and decimeter-scaled rocks located on the surface and/or rocks and voids within several radar wavelengths below the surface or any combination of these.

5. Delay-Doppler imaging

Delay-Doppler images from Arecibo and Goldstone are presented in Figs. 2 and 3. The imaging observations at Arecibo and Goldstone do not overlap because the rotation phases differ by more than 30° (Table 1). Due to time constraints at Arecibo, only 6 min were available for imaging before the target moved out of the observing window. 2005 WC1 appears somewhat irregular in shape with multiple facets and radar-bright areas in the Arecibo images. Two of the bright areas, labeled B1 and B2 on panel 8 of Fig. 2, could be localized elevated regions, boulders, facets, and/or regions with higher surface density which increases reflectivity. Although these areas could be caused by self-noise due to the small number of looks, it seems unlikely since they are consistently radar-bright. We summed the individual Arecibo images to create a single delay-Doppler image (Fig. 2b). The radar-bright features noted above and a possible radar-dark region near the receding edge then become more readily apparent.

On December 15 Goldstone imaged 2005 WC1 for 1.2 h and covered nearly 170° of rotation (Fig. 3). The echoes are very angular and confirmed the preliminary conclusion based on the Arecibo images that 2005 WC1 is an irregular object with multiple facets. Note that each image is fairly uniform in brightness from top to bottom. This uniformity is unusual for radar images which usually are much brighter along the edge that faces the observer. The echoes in panels 10, 11, and 12 in Fig. 3 look nearly trapezoidal. As the object rotates, the echoes take on a diamond-shaped appearance (panels 17 – 19) that is reminiscent of some radar images of 2003 MS2 (Lawrence et al., 2015), (4660) Nereus (Brozovic et al., 2009), (53319) 1999 JM8 (Benner et al., 2002), and (6489) Golevka (Hudson et al., 2000).

A face orthogonal to the radar line of sight returns a flat echo in time delay. The horizontal plane in panels 9–11 (labeled F1 in panel 10) of Fig. 3 has a maximum bandwidth of 4.6 Hz and corresponds to a length of 120 m if we adopt the 2.582 h rotation period. This facet rotates to the receding edge of the images in panels 20 and 21. The bandwidth of the horizontal plane labeled F2 in panel 19 in Fig. 3 is 5.5 Hz and corresponds to a length of 140 m. In addition, one can see an extension or bulge in panels 6 - 9 (labeled B1 in panel 7) on the receding side that reappear on the approaching side in panels 22 and 23. This extension is reminiscent of a feature seen on (53319) 1999 JM8 (Benner et al., 2002). By examining the rotation of these features, we estimate a rotation period of about 2.6 h, in agreement with the adopted rotational period of 2.582 ± 0.002 h.

A pronounced radar dark feature appears in the Goldstone images in panels 4 – 9 (Fig. 3). Although this could be interpreted as a radar albedo variation, a more likely explanation is a topographical feature such as a depression. One can see this feature rotate and become a “notch” on the receding side in panels 9 through 16, labeled D1 in panel 16.

We were unable to identify any surface features in the radar images that could cause the dip seen in the Goldstone echo power spectrum in Fig. 1, however, the object had rotated nearly 100 ° during the 42 min gap between the CW observations and imaging. Other radar-bright features can be seen in the delay-Doppler images (Figs. 2 and 3).

The dimensions of 2005 WC1 can be constrained further by counting the number of consecutive pixels in time delay that are at least 3-σ above the noise level. For a spherical object imaged at high signal-to-noise ratios, the visible extent corresponds to one half of the true extent. The visible extent of 2005 WC1 varies between 170 to 225 m in the Goldstone echoes and between 195 to 255 m in the echoes received at Arecibo. If we assume that we see only one half of the true extent, then the maximum length of the largest dimension is about 510 m. This is inconsistent with the 0.29 km diameter estimated by Trilling et al., (2010) and is much larger than the lower bounds implied by the bandwidths and rotation period determined from Arecibo and Goldstone (0.17 and 0.23 km, respectively). However, interpreting the visible extent in this manner is complicated by the angularity of the object and the projection of several pixels of the echo power at the trailing edges of the echoes (at both negative and positive frequencies) in Fig. 3. In addition, an object with a diameter of 0.51 km and rotation period of 2.582 h would yield a bandwidth, as seen from Goldstone, of nearly 20 Hz if viewed equatorially. The Goldstone and Arecibo diameters estimated from doubling the visible extent averages are 390 and 434 m, respectively, so we adopt 400 ± 50 m (where the uncertainty is 1σ) as our best estimate. This is a rough estimate because the data do not provide sufficient rotational coverage and sky motion to estimate a unique 3D shape model.

Pravec and Harris (2007) established a relationship between the absolute magnitude, H, the diameter of the target, D, and the geometric albedo, p_v, that can be expressed as:

$$D\sqrt{p_v} = 1329 \times 10^{-H/5}. \quad (2)$$

Using this expression and adopting the diameter, D = 0.40 km, estimated from the visible extents, we obtain an optical albedo of 0.06, implying that 2005 WC1 is optically dark and most likely not an E-type or V-type asteroid. Optical albedos are available for three of the five known X-type NEAs with high circular polarization ratios listed in Table 4. These values are 0.72 (+0.31, −0.25) for (17511) 1992 QN (Thomas et al., 2011); 0.24 (+0.25, −0.11) for (141593) 2002 HK12 (Wolters et al., 2005) and 0.408 ± 0.061 for (163132) 2002 CU11 (Mainzer et al., 2011). None of these would be considered dark. Even if we adopt the diameter of 0.29 km reported by Trilling et al. and H = 20.7, then we obtain an optical albedo of 0.11 that is much lower than expected for any E- or V-class NEA. If 2005 WC1 truly has a low optical albedo, then it probably is not a member of the E or V spectral classes, both of which tend to be optically bright. Consequently, 2005 WC1 may be the first NEA with SC/OC > 1 that can not be one of these two classes.

If we were to adopt D = 0.20 km as estimated from the average bandwidths as a lower bound, then we obtain an upper bound

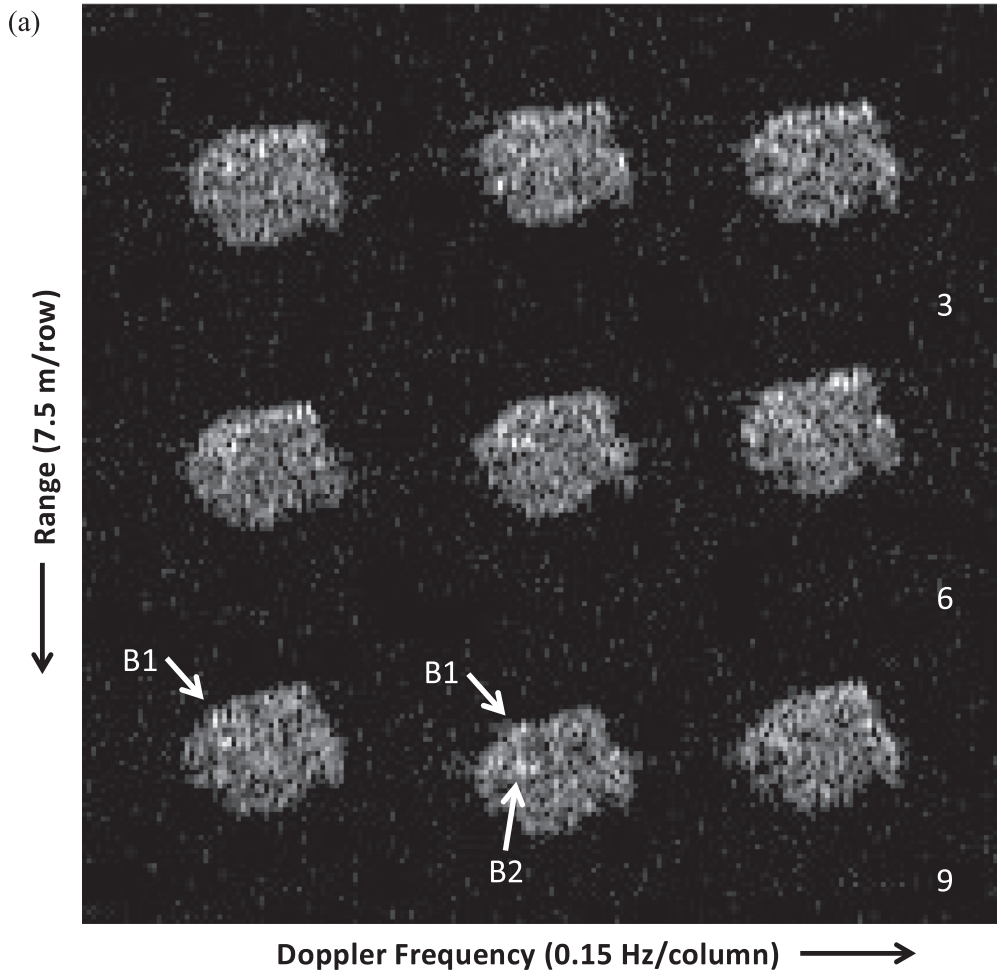

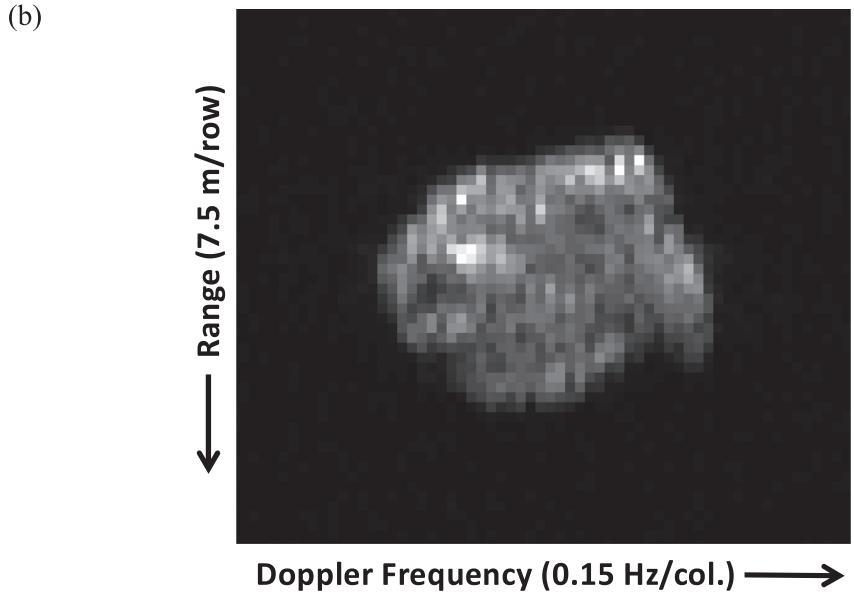

Fig. 2. (a) Delay-Doppler radar images of 2005 WC1 acquired on December 14 at Arecibo between 14:44:13 – 14:50:20 UTC. Range increases downward and Doppler frequency increases towards the right so that the rotation appears counter-clockwise. Time increases toward the right and downward. Each image shows one run. The images drift in time delay. This "jitter" is a result of the ephemeris shifting because the echo in range was roughly constant during the short sequence of images. Arrows indicate features discussed in the text. (b) Summed image of the nine individual Arecibo delay-Doppler images. The "jitter" seen in Fig. 2a is compensated by taking into account the difference in the pixel location of the ephemeris reference point in each image and shifting them to a common reference position. The asteroid rotated 14° during this time period. Details including radar-bright and radar-dark features become more apparent.

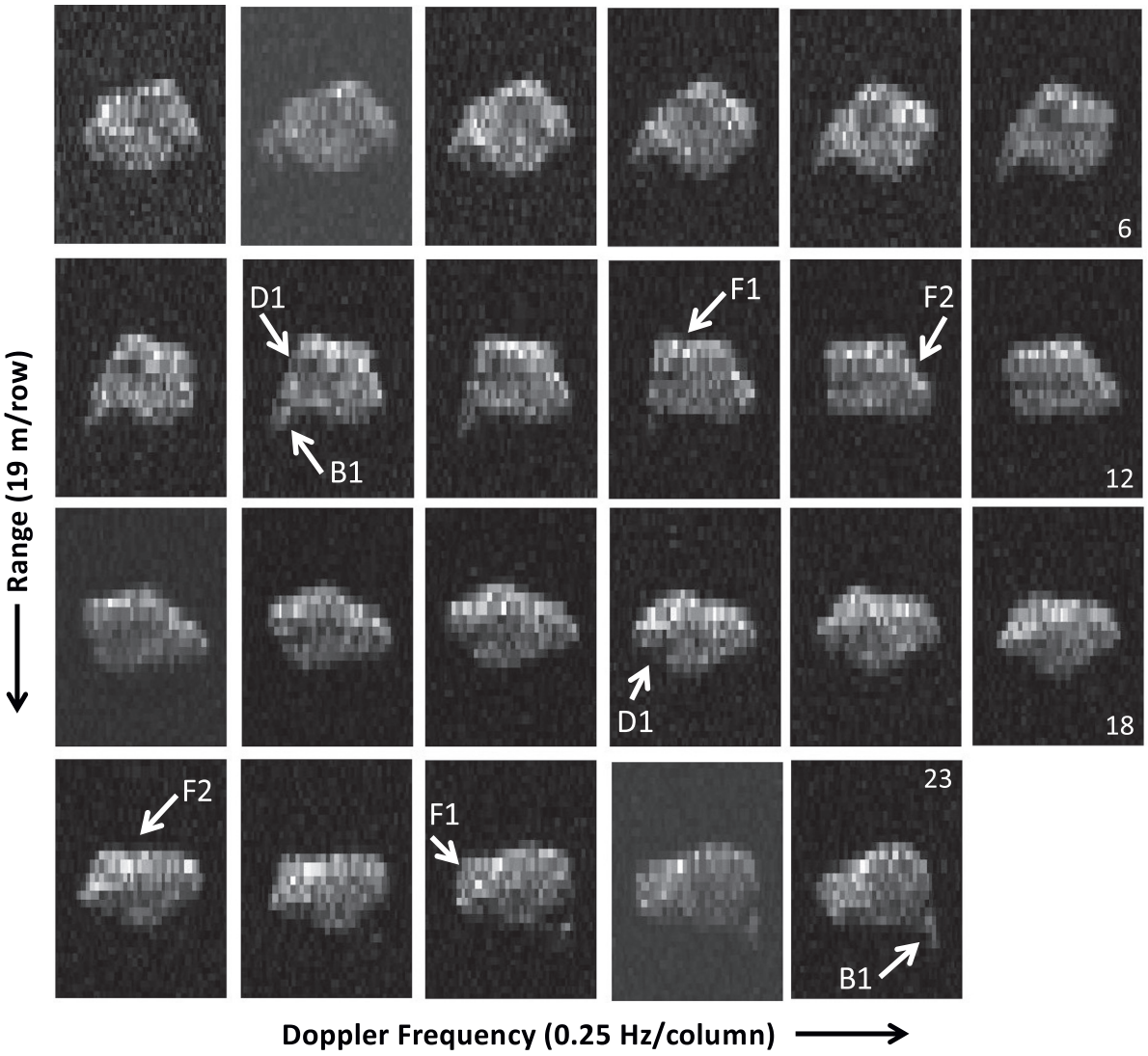

Fig. 3. Goldstone delay-Doppler radar images acquired on December 15 between 14:12:08 – 15:30:07 UTC. Image orientation is the same as in Fig. 2 and do not exhibit any "jitter" as seen in the Arecibo images. Each image is a sum of four runs. The arrows indicate features discussed in the text.

Table 4
Near-Earth Asteroids with the highest circular polarization ratios.

Rank	Object	SC/OC	Obs	Year	H	Class	Reference
1 (348400)	2005 JF21	1.57 ± 0.38	A	2015	17.3	V	Howell (pers. comm.)
2	2003 TH2	1.48 ± 0.04	A	2003	22.8	?	Benner et al. (2008)
3	2013 PR43	1.46 ± 0.05	A	2013	23.4	?	
4	2010 CF19	1.40 ± 0.013	A	2013	21.7	?	
5 (189008)	1996 FR3	1.21 ± 0.5	A	2015	16.3	?	
6 (416151)	2002 RQ25	1.19 ± 0.021	A	2015	20.6	C/X	Thomas et al. (2014)
7	2009 DL46	1.16 ± 0.004	A	2016	22.0	?	
8 (469896)	2005 WC1	1.12 ± 0.05	G	2005	20.7	?	This work
9 (382758)	2003 GY	1.11 ± 0.15	A	2003	20.2	?	Benner et al. (2008)
10 (17511)	1992 QN	1.10 ± 0.19	G	1996	17.1	X	Benner et al. (1997), Benner et al. (2008)
11 (138175)	2000 EE104	1.1 ± 0.3	A	2000	20.3	X	Howell et al. (2001), Benner et al. (2008)
12 (141593)	2002 HK12	1.09 ± 0.06	A	2002	18.1	X	Benner et al. (2008)
13 (443103)	2013 WT67	1.05 ± 0.02	A	2017	18.0	?	
14 (443880)	2001 UZ16	1.04 ± 0.04	A	2015	19.4	?	
15 (2101)	Adonis	1.02 ± 0.11	A	1984	18.8	?	Benner et al. (1997), Benner et al. (2008)
16	2005 TU50	1.02 ± 0.15	A	2005	21.4	?	Benner et al. (2008)
17	2001 BB16	1.02 ± 0.032	A	2016	23.1	?	
18 (163132)	2002 CU11	1.01 ± 0.2	A	2014	18.5	C/X	Thomas et al. (2014)
19	2002 VE68	1.0 ± 0.2	G	2002	20.5	X	Benner et al. (2008), Hicks et al. (2010)

NEAs with circular polarization ratios above unity observed from Arecibo (A) and Goldstone (G). The year of the observations, the absolute magnitude, H, and taxonomic class are provided. References provide previously published circular polarization ratios, if available.

Table 5
Disk-integrated radar properties.

Date	μ_c	σ_{oc} (km^2)	λ (cm)
2005-Dec-14	N/A	0.07 ± 0.02	12.6
2005-Dec-15	1.12 ± 0.05	0.03 ± 0.01	3.5

Circular polarization ratios, μ_c, and OC radar cross-sections, σ_{oc}, obtained on each day of the radar experiment.

of 0.23 for the optical albedo. This moderate albedo is consistent with an S, Q, M or V-type object. However, the measured polarization ratio of 1.12 is much higher than any other member of the S or M class, which have means of 0.27 and 0.14, respectively (Benner et al., 2008). The highest previously observed polarization value of an S-class member is 0.50 (Benner et al., 2008). In fact, no object in the Benner et al. (2008) study with a taxonomic class inconsistent with E or V has a polarization ratio greater than 0.55.

Juric et al. (2002) reported a systematic shift with the MPC catalog H-magnitudes of ∼0.4 magnitudes. Pravec et al. (2012) also found that the MPC H-magnitudes were too bright by evaluating WISE data and Veres et al. (2015) agreed with their results using the larger Pan-STARRS dataset. Generally, the H-magnitude offsets are small with larger asteroids (H $\sim<$ 10) depending on the orbital catalog. If the absolute magnitude of 20.7 reported by the Minor Planet Center and the JPL/Horizons online ephemeris system is too bright by 0.4 magnitudes, then the optical albedo values may decrease as much as thirty percent, which would bolster the conclusion that 2005 WC1 is optically dark. In order to obtain optical albedo values within the range reported for E- or V-class objects (i.e. $\sim>$ 0.3), and assuming that D = 0.4 km, the absolute magnitude would need to be brighter than H = 19, which seems very unlikely.

The opposite-sense radar albedo, $\hat{\sigma}_{OC}$, is defined as:

$$\hat{\sigma}_{OC} = \sigma_{OC}/A = 4\sigma_{OC}/\pi D_{eff}^2 \quad (3)$$

where A is the asteroid's projected area and D_{eff} is the effective diameter of a sphere with the same projected area as the object. Table 5 summarizes the radar properties. Using D = 0.40 km and the Goldstone radar cross-section from Table 5, we obtain a lower bound for the radar albedo of 0.24 that is slightly above the average value of 0.20 ± 0.12 from a population of 40 asteroids (see http://echo.jpl.nasa.gov/∼lance/asteroid_radar_properties/nea.radaralbedo.html). We obtain a radar albedo of 0.56 using the Arecibo cross-section, which seems very high and implies an almost pure iron-nickel object. The only NEA known to have such a high albedo is (6178) 1986 DA (Ostro et al., 1991).

The different radar cross-sections and albedos may be explained by several factors. First, the radar cross-section can be dependent upon the frequency of the radar transmitter, although in practice significant differences among NEAs seem to be rare. Secondly, systematic calibration and pointing errors contribute uncertainties in the radar cross-section of approximately 35% at Goldstone and 25% at Arecibo. More likely, viewing an irregularly-shaped object can produce a different cross-section depending on the orientation. 2005 WC1's large surface facets may contribute to the differing cross-sectional values. For example, a large 100 m-scale sections act like mirrors reflecting the radar and can give a high cross section compared to a facet that is angled away from the line of sight.

In addition, the Arecibo data provides only a brief snapshot of a highly angular, rapidly- rotating object that cannot be taken as representative of the whole object.

6. Discussion

The dynamic range in SNRs between the leading and trailing edges of the Goldstone images is substantially less than we observe for other NEAs imaged by radar. The unusually uniform brightness of the radar images suggests extreme roughness, as there is less visible scattering at the sub-Earth point than is usually evident with most other NEAs imaged by Arecibo or Goldstone. 2005 WC1 was the first NEA with a high circular polarization ratio imaged in detail, so perhaps it should not be surprising that its radar scattering properties are different from NEAs with significantly lower polarization ratios. To date, several other NEAs with high polarization ratios have subsequently been imaged and a future paper will investigate if the appearance of their images is truly different.

Benner et al. (2008) found that the average circular polarization ratio of 214 near-Earth asteroids is 0.34 ± 0.25. With an SC/OC ratio of 1.12 ± 0.02, a factor of three higher than the average, it suggests that 2005 WC1 is much more rough than objects that have been visited by spacecraft such as Itokawa (μ_c = 0.26 ± 0.04; Ostro et al., 2004), Eros (μ_c = 0.28 ± 0.06; Magri et al., 2001), and Toutatis (μ_c = 0.29 ± 0.01; Ostro et al., 1999).

Polarization ratios greater than unity have been observed on other bodies including glaciers on the Earth, the polar ice caps on Mars, and some outer planet satellites where the high polarization ratios are attributed to "coherent backscatter" from thick layers of water ice (e.g., Ostro, 1993). While this is physically conceivable for 2005 WC1, it seems quite unlikely, as one would expect cometary activity from an object with significant water ice as close to the sun as 2005 WC1. Furthermore, no optical observers reported cometary activity that most likely would have been visible during the close 2005 apparition. Why does 2005 WC1 have a high circular polarization ratio and a low optical albedo? This combination of surface properties is distinctly unlike any other near-Earth or main-belt asteroid studied in detail to date. Virkki et al. (2014) and Virkki and Muinonen (2016) modeled the effects of radar scattering by planetary surfaces using laboratory particles to investigate the causes of high circular polarization ratios. From their study, objects with a high polarization ratio and radar albedo imply a high number density of wavelength-scale scattering particles on the surface or a short distance below it, possibly coupled with high metal content (Virkki and Muinonen, 2016). Virkki and Muinonen (2016) found computed circular polarization ratios were higher for irregular particles than for spherical particles and that coherent backscattering increases SC/OC as well as the radar albedo. Interpretations from their model suggest asteroids with high circular polarization ratios are solid objects or covered with a fine-grained regolith. Optically dark asteroids have not previously shown high circular polarization ratios but there does not appear to be any particular reason a priori why surfaces exhibiting these properties cannot exist. The lack of previous detections hints that surfaces producing there properties are uncommon within the optically-dark spectral classes.

Although the spectral class of 2005 WC1 is unknown, twelve of the twenty-six objects (46%) in the Benner et al. (2008) study with SC/OC greater than 0.6 belong to the E, V, or X classes. The spectral classes of the remaining objects in the study are unknown. Since the Benner et al. (2008) study, numerous other NEAs with high circular polarization ratios have been observed and all with known spectral classes are in the E-, V-, or X-classes. However, the optical albedo of 2005 WC1 is too low to belong to the E and V classes, but the X-class is degenerate and includes E-, M-, and P-types, and of these, the P-class objects have low optical albedos, so perhaps 2005 WC1 has a P-type taxonomy.

Since the Benner et al. (2008) publication, nearly 500 additional near-Earth asteroids have been observed with radar at Arecibo and Goldstone. Table 4 lists all the objects with circular polarization ratios greater than unity observed as of May 2017. The highest value, SC/OC = 1.57, was measured for (348400) 2005 JF21 (http://www.naic.edu/∼pradar/asteroids/2005JF21/2005JF21.2015Jul23.s0p38Hz.cw.png). 2005 WC1 ranks

eighth. Of these nineteen objects, five (26%) are in the X class, so they could be members of the E, M, or P classes.

7. Future observations

The next flyby close enough for radar observations will occur in December 2068 at 0.065 au. Radar facilities operating with the current capabilities of Arecibo and Goldstone could achieve daily signal-to-noise ratios of 330 and 16, respectively. During this close approach, 2005 WC1 will be at an approximate visual magnitude of 18.0 and a solar elongation of 90°. The next encounter closer than this will be at 0.036 au in December 2126. Prior to 2068, there are several opportunities for optical observers to obtain lightcurves to constrain the pole position and/or spectroscopy to determine the taxonomic class. Two optimal apparitions occur in 2034 and 2039 when the object will reach a visual magnitude of at least 18.5.

Acknowledgments

We thank the technical and support staffs of Goldstone and Arecibo for their assistance with the observations. Comments by Chris Magri and an anonymous reviewer improved the manuscript. A portion of this research was conducted at the Jet Propulsion Laboratory, California Institute Technology, under contract with the National Aeronautics and Space Administration (NASA). The Arecibo Observatory is part of the National Astronomy and Ionosphere Center (NAIC), which at the time of these observations was operated by Cornell University under a cooperative agreement with the National Science Foundation (NSF). The material presented represents work supported by NASA under the Science Mission Directorate Research and Analysis Programs.

References

Benner, L.A.M., Ostro, S.J., Giorgini, J.D., Jurgens, R.F., Mitchell, D.L., Rose, R., Rosema, K.D., Slade, M.A., Winkler, R., Yeomans, D.K., Campbell, D.B., Chandler, J.F., Shapiro, I.I, 1997. Radar detection of near-Earth asteroids 2062 Aten, 2101 Adonis, 3103 Eger, 4544 Xanthus, and 1992 QN. Icarus 130, 296–312.

Benner, L.A.M., Ostro, S.J., Nolan, M.C., Margo, J.L., Giorgini, J., Hudson, R.S., Jurgens, R.F., Slade, M.A., Howell, E.S., Campbell, D.B., Yeomans, D.K., 2002. Radar observations of asteroid 1999 JM8. Meteorit. Planet. Sci. 37, 779–792.

Benner, L.A.M., Ostro, S.J., Magri, C., Nolan, M.C., Howell, E.S., Giorgini, J.D., Margot, J.L., Busch, M.W., Shepard, M.K., Taylor, P.A., Jurgens, R.F., 2008. Near-Earth asteroid surface roughness depends on compositional class. Icarus 198, 294–304.

Brozovic, M., Ostro, S.J., Benner, L.A.M., Giorgini, J.D., Jurgens, R.F., Rose, R., Nolan, M.C., Hine, A.A., Magri, C., Scheeres, D.J., Margot, J.L., 2009. Radar observations and a physical model of asteroid 4660 Nereus, a prime space mission target. Icarus 201, 153–166.

Brozovic, M., Benner, L.A.M., Magri, C., Ostro, S.J., Scheeres, D.J., Giorgini, J.D., Nolan, M.C., Margot, J.L., Jurgens, R.F., Rose, R., 2010. Radar observations and a physical model of contact-binary asteroid 4486 Mithra. Icarus 208, 207–220.

Hicks, M., Mayes, D., Barajas, T., 2010. Broadband photometry of 2002 VE68, a quasi-moon of Venus. Astronomer's Telegram, ATel #3073.

Higley, S., Hardersen, P., Dyvig, R., 2008. Do what you can photometry: unfiltered photometry of NEOs 2005 PJ2, 2005 WC1, and 2006 GY2. Minor Planet Bull. 35, 175–177.

Howell, E.S., Nolan, M.C., DeRemer, L., Margot, J.L., 2001. Arecibo radar observations of near-Earth asteroid 2000 EE104. Bull. Am. Astron. Soc. 33, 1153.

Hudson, R.S., Ostro, S.J., Jurgens, R.F., Rosema, K.D., Giorgini, J.D., Winkler, R., Rose, R., Choate, D., Cormier, R.A., Franck, C.R., Frye, R., Howard, D., Kelley, D., Littlefair, R., Slade, M.A., Benner, L.A.M., Thomas, M.L., Mitchell, D.L., Chodas, P.W., Yeomans, D.K., Scheeres, D.J., Palmer, P., Zaitsev, A., Koyama, Y., Nakamaura, A., Harris, A.W., Meshkov, M.N., 2000. Radar observations and physical model of asteroid 6489 Golevka. Icarus 148, 37–51.

Juric, M., Ivezic, Z., Lupton, R.H., Quinn, T., Tabachnik, S., Fan, X., Gunn, J.E., Hennessy, G.S., Knapp, G.R., Munn, J.A., Pier, J.R., Rockosi, C.M., Schneider, D.P., Brinkmann, J., Csabai, I., Fukugita, M., 2002. Comparison of positions and magnitudes of asteroids observed in the Sloan Digital Sky Survey with those predicted for known asteroids. Astron. J. 124, 1776–1787.

Lawrence, K.J., Benner, L.A.M., Brozovic, M., Ostro, S.J., Jao, J., Giorgini, J., Slade, M., Jurgens, R.F., 2015. Goldstone radar imaging of near-Earth asteroid 2003 MS2. Icarus 260, 1–6.

Magri, C., Consolmagno, S.J., Ostro, S.J., Benner, L.A.M., Beeney, B.R., 2001. Radar constraints on asteroid regolith properties using 433 Eros as ground truth. Meteorit. Planet. Sci. 36, 1697–1709.

Magri, C., Howell, E.S., Nolan, M.C., Taylor, P.A., Fernandez, Y.R., Mueller, M., Vervack Jr., R.J., Benner, L.A.M., Giorgini, J.D., Ostro, S.J., Scheeres, D.J., Hicks, M.D., Rhoades, H., Somers, J.M., Gaftonyuk, N.M., Kouprianov, V.V., Krugly, Y.N., Molotov, I.E., Busch, M.W., Margot, J.L., Benishek, V., Protitch-Benishek, V., Galad, A., Higgins, D., Kusnirak, P., Pray, D.P., 2011. Radar and photometric observations and shape modeling of contact binary near-Earth asteroid (8567) 1996 HW1. Icarus 214, 210–227.

Mainzer, A., Grav, T., Bauer, J., Masiero, J., McMillan, R.S, Cutri, R.M., Walker, R., Wright, E., Eisenhardt, P., Tholen, D.J., Spahr, T., Jedicke, R., Denneau, L., DeBaun, E., Elsbury, D., Gautier, T., Gomillion, S., Hand, E., Mo, W., Watkins, J., Wilkins, A., Bryngelson, G.L., Del Pino Molina, A., Desai, S., Gomez Camus, M., Hidalgo, S.L., Konstantopoulos, I., Larsen, J.A., Maleszewski, C., Malkan, M.A., Mauduit, J.-C., Mullan, B.L., Olszewski, E.W., Pforr, J., Saro, A., Scotti, J.V., Wasserman, L.H., 2011. NEOWISE observations of near-Earth objects: preliminary results. ApJ 743, 156.

Miles, R, 2008. The 2007 BAA presidential address: asteroids: past, present and future. BJAA 118, 187–198.

Ostro, S.J., Campbell, D.B., Chandler, J.F., Hine, A.A., Hudson, R.S., Rosema, K.D., Shapiro, I.I., 1991. Asteroid 1986 DA: radar evidence for a metallic composition. Science 252, 1399–1404.

Ostro, S.J., 1993. Planetary radar astronomy. Rev. Modern Phys. 65, 1235–1279.

Ostro, S.J., Hudson, R.S., Rosema, K.D., Giorgini, J.D., Jurgens, R.F., Yeomans, D.K., Chodas, P.W., Winkler, R., Rose, R., Choate, D., Cormier, R.A., Kelley, D., Littlefair, R., Benner, L.A.M., Thomas, M.L., Slade, M.A., 1999. Asteroid 4179 Toutatis: 1996 radar observations. Icarus 137, 122–139.

Ostro, S.J., Benner, L.A.M., Nolan, M.C., Magri, C., Giorgini, J.D., Scheeres, D.J., Broschart, S.B., Kaasalainen, M., Vokrouhlicky, D., Chesley, S.R., Margot, J.L., Jurgens, R.F., Rose, R., Yeomans, D.K., Suzuki, S., de Jong, E.M., 2004. Radar observations of asteroid 25143 Itokawa (1998 SF36). Meteorit. Planet. Sci. 39, 407–424.

Pravec, P., Harris, A.W., 2007. Binary asteroid population 1. Angular momentum content. Icarus 190, 250–259.

Pravec, P., Harris, A.W., Kusnirak, P., Galad, A., Hornoch, K., 2012. Absolute magnitudes of asteroids and a revision of asteroid albedo estimates from WISE thermal observations. Icarus 221, 365–387.

Shepard, M.K., Clark, B.E., Ockert-Bell, M., Nolan, M.C., Howell, E.S., Magri, C., Giorgini, J.D., Benner, L.A.M., Ostro, S.J., Harris, A.W., Warner, B.D., Stephens, R.D., Mueller, M., 2010. A radar survey of M- and X-class asteroids II. Summary and synthesis. Icarus 208, 221–231.

Thomas, C.A., Trilling, D.E., Emery, J.P., Mueller, M., Hora, J.L., Benner, L.A.M., Bhattacharya, B., Bottke, W.F., Chesley, S., Delbo, M., 2011. ExploreNEOs V. Average albedo by taxonomic complex in the near-Earth asteroid population. Astron. J. 142, 85.

Thomas, C.A., Emery, J.P., Trilling, D.E., Delbo, M., Hora, J.L., Mueller, M., 2014. Physical characterization of warm Spitzer-observed near-Earth objects. Icarus 228, 217–248.

Trilling, D.E., Mueller, M., Hora, J.L., Harris, A.W., Bhattacharya, B., Bottke, W.F., Chesley, S., Delbo, M., Emery, J.P., Fazio, G., Mainzer, A., Penprase, B., Smith, H.A., Spahr, T.B., Stansberry, J.A., Thomas, C.A, 2010. ExploreNEOs. I. Description and first results from the warm Spitzer near-Earth object survey. Astron. J. 140, 770–784.

Veres, P., Jedicke, R., Fitzsimmons, A., Dennaeu, L., Granvik, M., Bolin, B., Chastel, S., Wainscoat, R.J., Burgett, W.S., Chambers, K.C., Flewelling, H., Kaiser, N., Magnier, E.A., Morgan, J.S., Price, P.A., Tonry, J.L., Waters, C., 2015. Absolute magnitudes and slope parameters for 250,000 asteroids observed by Pan-STARRS PS1 – Preliminary results. Icarus 261, 34–47.

Virkki, A., Muinonen, K., Penttila, A., 2014. Inferring asteroid surface properties from radar albedos and circular-polarization ratios. Meteor. Planet. Sci. 49, 86–94.

Virkki, A., Muinonen, K., 2016. Radar scattering by planetary surfaces modeled with laboratory-characterized particles. Icarus 269, 38–49.

Vokrouhlicky, D., Farnocchia, D., Capek, D., Chesley, S.R., Pravec, P., Scheirich, P., Muller, T.G., 2015. The Yarkovsky effect for 99942 Apophis. Icarus 252, 277–283.

Wolters, S.D., Green, S.F., McBride, N., Davies, J.K., 2005. Optical and thermal infrared observations of six near-Earth asteroids in 2002. Icarus 175, 92–110.